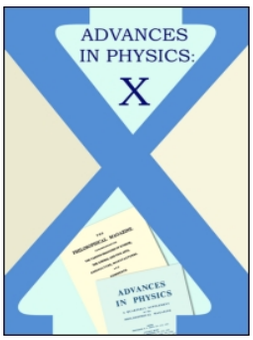

Advances in Physics: X

ISSN: (Print) 2374-6149 (Online) Journal homepage: https://www.tandfonline.com/loi/tapx20

Precipitates in aluminium alloys

Sigmund J. Andersen, Calin D. Marioara, Jesper Friis, Sigurd Wenner & Randi Holmestad

To cite this article: Sigmund J. Andersen, Calin D. Marioara, Jesper Friis, Sigurd Wenner & Randi Holmestad (2018) Precipitates in aluminium alloys, Advances in Physics: X, 3:1, 1479984, DOI: 10.1080/23746149.2018.1479984

To link to this article: https://doi.org/10.1080/23746149.2018.1479984

Published online: 07 Aug 2018.

ADVANCES IN PHYSICS: X
2018, VOL. 3, NO. 1, 1479984
https://doi.org/10.1080/23746149.2018.1479984

Taylor & Francis
Taylor & Francis Group

REVIEW ARTICLE

OPEN ACCESS Check for updates

Precipitates in aluminium alloys

Sigmund J. Andersen[a], Calin D. Marioara[a], Jesper Friis[a], Sigurd Wenner[a] and Randi Holmestad[b]

[a]Sintef Industry, Department of Materials and Nanotechnology, Trondheim, Norway; [b]Norwegian University of Science and Technology (NTNU), Department of Physics, Trondheim, Norway

ABSTRACT

Precipitation strengthening is a highly complex phenomenon on the nanoscale, responsible for providing strength in Al-Cu, Al-Mg-Cu, Al-Mg-Zn and Al-Mg-Si alloys. Advances in methodology, especially high-angle annular dark-field transmission electron microscopy and atomistic calculations provide fundamental insights into the mechanisms behind precipitation. We are beginning to understand how solute elements form precipitates from the Al matrix and how structures relate. Examples are Ω, η' and η-phases of Al-Cu and Al-Mg-Zn, where solute organizes in similar supercells in the aluminium lattice. In Al-Mg-Si and Al-Mg-Cu, discovery of 1D Guinier–Preston zone aids understanding of precipitation and growth in the two systems.

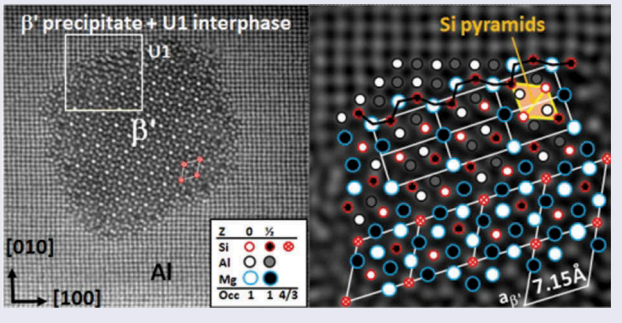

Abbreviation: 1D: one-dimensional, 3D: three-dimensional, Cs – probe: Spherical aberration corrected electron probe, DFT: Density functional theory, eV: Electron volt, FCC: Face centred cubic, FEG: Field emission gun, GP: Guinier-Preston, GPB: Guinier-Preston-Bagaryatsky, HAADF: High angle annular dark-field, ISMEAR: First order Methfessel-Paxton for smearing, NN: Nearest neighbour, Occ: Occupancy, PAW: Projector augmented wave method, PBE: Perdew-Burke-Enzerhof, STEM: Scanning transmission electron microscopy, TEM: Transmission electron microscopy.

ARTICLE HISTORY
Received 5 January 2018
Accepted 17 May 2018

KEYWORDS
HAADF-STEM; DFT calculations; GP- zones; crystal structures; precipitates; aluminium alloys

PACS
61.25.Mv (for 'structure of alloys'); 71.15.Mb (for DFT calculations); 68.37.Og (For HRTEM); 68.37.-d (Structure determination by electron microscopy); 81.40.Cd (for Precipitation hardening/aging)

CONTACT Sigmund J. Andersen Sigmund.J.Andersen@sintef.no

Introduction

Aluminium and discovery of precipitation/age-hardening

Aluminium is the most common metal in the earth's crust [1], its production ranks second only to iron. The primary production in 2016 was 60 million metric tonnes [2], using 3% of the world electric supply. Initially more expensive than gold, aluminium became a commodity around 1900. Poor strength was a problem. In 1909, Alfred Wilm patented Duralumin – the first age-hardened aluminium alloy, containing about 4 Cu, 0.5–1.5 Mg and 0.5–1 Mn (wt%) [3,4], which more than doubled the strength. Recent analyses found that the Wright brothers already had enjoyed the strengthening benefits for the first flight in 1903, since the aircraft engine parts used cast Al-8%Cu, which had been age-hardened, although probably inadvertently [5].

Small amounts of solute elements like Mg, Si, Cu and Zn define the various alloy systems. To optimise and prevent failures, products are manufactured according to strict procedures and heat treatments (c.f. [6,7]). Getting precipitation wrong is easy, as both processing and temperature history influence the small precipitates that are responsible for the hardening.

A first step is dissolving the solute in Al in the single-phase region. Figure 1 shows the Al-side of the Al-Cu phase diagram [8], which can represent the general precipitation-hardened alloy. The circle shows that for an Al-3.5Cu alloy, all Cu dissolves at 550°C. Max solubility is 5.65%, while just 0.04% Cu dissolves in Al at room temperature (RT). The shaded

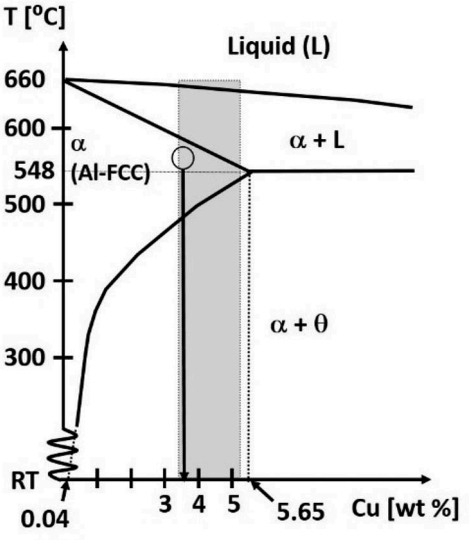

Figure 1. Al-side of the Al-Cu phase diagram [8]. Fast cooling of Al-3.5% Cu alloy from single-phase 03B1 region (arrow) creates a large supersaturation of Cu at RT, whereby precipitates can form. Grey region indicates Cu amount in Duralumin alloys.

area shows the Cu limits for Duralumin. Fast cooling to RT freezes the high-temperature state, preventing the *equilibrium* θ-Al_2Cu from forming, rendering the alloy in *supersaturated solid solution* (SSSS). This state is highly unstable even at RT. Initially, Cu atoms diffuse and form ordered regions caller Guinier-Preston (GP) zones. With time and higher temperature metastable *precipitates*are observed. Higher temperature and time produce θ-Al_2Cu - a structure determined in 1927 by Friauf [9] and confirmed by single-crystal X-ray diffraction [10].

Vacancies

To form precipitates, vacancies are required. The SSSS comprises excess solute and vacancies. Experiments and calculations estimate 1 vacancy per 100 solute atoms at 550°C [11]. At a typical ageing temperature (185°C), this fraction reduces to ~10^{-5}, and to 10^{-10} at RT. Quenching from 550°C produces a tremendous vacancy surplus at RT, increasing diffusion. As a result, solute clusters form at RT, which can be verified by a slowly increasing hardness [12] – a process called *natural ageing*. Vacancies may form clusters [13] and dislocation loops [14–16]. They attract solute and result in coarser, fewer particles, an effect which lowers strength, and can be severe in alloys [17] low in solute. Some elements attract vacancies, thereby 'catalysing' nucleation [18,19]. For example, first principle calculations find binding energy to increase as Cr, Mn, Li, Fe, Mg, Al, Cu, Zn, Si and Ge [19,20]. It is therefore not surprising that Si and Ge increase precipitation of θ' in Al-Cu alloys [19,21,22]. Ge in Al-Mg-Si increases strength by giving higher numbers of finer precipitates [23,24].

Atomic size, solid solution, strengthening and ordering

Solute atoms are lattice defects in Al, causing local strain and (solute) hardening. As shown by first principle calculations, Si, Cu and Zn are smaller atoms in Al, causing local contraction in aluminium, while Mg and Ge expand it [19,20]. It suggests that the difference in local strain energy can be reduced by smart arranging of small and large atoms. As explained in the following, strain alleviating arrangements may explain many of the early precipitates in Al-Mg-Cu and Al-Mg-Si [25–29]. Although solute strengthening is important, such as in Cu-Sn alloys (which came to define the Bronze Age [30]), it is a secondary mechanism in precipitation-hardened alloys. However, it is exploited in the Al-Mg (5xxx) alloys, where near 6 wt% Mg can dissolve [31]. The expansion or contraction in solid solution was originally believed to be linearly dependent as predicted by *Vegard's law* [32], but the law represents the exception [33]. For example, Mg exhibits complex solute orderings that are not well understood. In Al-Mg alloys, Sato

reported a specific ordering in Al, called $L1_2$, as well as directed solute concentration waves called *spinodal decomposition* [34]. The ordering is likely to interact with the precipitation processes at the nanoscale.

The phases in the equilibrium-phase diagram

Precipitates are typically *metastable* and cannot exist outside the Al lattice. In Al-Cu, the θ-Al_2Cu phase is stable. Slow cooling can lead to large particles. Larger, second phases nearly always constitute a problem. They reduce the potential of the solute and can give corrosion problems in grain boundaries [35]. Al-Si alloys (with the only second phase of silicon in diamond structure) are often considered an exception. The alloys are popular for the automotive and aerospace applications [36] and the 3D printing technologies.

From SSSS to equilibrium phases – a sequence of metastable precipitates

Decomposition of the SSSS state takes several stages. By combining atom probe microscopy, positron lifetime measurements and microscopy on the RT-stored Al-Mg-Si alloys [12], it was suggested Si forms initial clusters, attracting slower Mg atoms, causing co-clusters to form, which then further grow into Guinier–Preston (GP)-zones. Calculations of semi-cells of β'' (structurally close to GP-zones) support this [37]. The zones are replaced by a sequence of metastable, semi-coherent phases, with lower energy. Gradually, as coherency with Al is lost, precipitates become fewer, larger and may turn into the incoherent stable particles. It is seen as their shapes become more equiaxed.

Methodology

For results described here, high angle annular dark-field-scanning transmission electron microscopy (HAADF-STEM) images were obtained in a spherical aberration CS-probe corrected JEOL ARM200F, with a cold field emision gun (FEG) at 200 kV high voltage, probe size 0.08 nm and an inner collector angle 50 mrad. Precipitates are shown in aluminium zones <100> and <211>.

Density functional theory (DFT) is very important for understanding solute behaviour and phase stability [38–44]. We show calculations of energy change from arbitrary solid solution of Mg, Si and Cu to ordered 1D, infinite GP-zone in the Al matrix. The Al lattice parameter used for the calculations is based on a relaxed $4 \times 4 \times 1$ unit (64 atoms) aluminium supercell (at zero Kelvin). The Vienna *ab initio* simulation package [40,41] was employed for DFT calculations [42,43], using the projector-augmented wave method within the PBE generalized gradient approximation. The plane-wave energy cut-off was 400 eV. For all calculations, gamma-centred

k-points were used, with maximal k-point distances of 0.25 $Å^{-1}$ in each direction. The electronic accuracy for self-consistent loops was set at 10^{-6} eV. The atomic positions were relaxed to a maximal force of 0.001 eV/Å between atoms using first-order Methfessel-Paxton for smearing of partial occupation (ISMEAR) and a smearing factor (SIGMA) of 0.2. Separate calculations were performed for more accurate energies using the tetrahedron method with Blöchl correction for the smearing.

Precipitates in Al-Cu-(Mg/Zn) alloys

For Al-Cu, the sequence of precipitation phases is given as [5,44–46]:

$$\text{SSSS} \rightarrow \text{solute clusters} \rightarrow \text{GP1} \rightarrow \text{GP2}(\text{q}'') \rightarrow \text{q}' \rightarrow \text{q} = \text{Al}_2\text{Cu}$$

In principle, the GP-zone structure in binary Al-Cu alloys is simple: Cu replaces Al atoms in a region of a {100} plane called 'GP1' or 'GP-I' zone [5]. Figure 2 shows that such GP-zone is not unique to the binary Al-Cu alloys: Here, it forms in the alloy Al-0.7Mg–0.8Si with 0.5 wt% Cu, which was heated 15 min at 200°C. At the Cu plane, a (screw) dislocation can be seen. That such planes exist in Al-Cu alloys [46] means they are stable without Mg.

The second phase in the precipitation sequence is the GP-II zone (θ''). Ideally Al_3Cu, it consists of two or more Cu planes in parallel (separation 4 = 8.1 Å), i.e. replacing every fourth Al-plane [46–48]. Atom probe experiments [44,49] and recent calculations find less than expected Cu [44], meaning the GP-II structure is unclear. Figure 3 (lower right) shows an example of a GP-II zone. A recent work detected Cu ordering also between the Cu planes [50]. Monte Carlo *ab-initio* bulk simulations in dilute Al-Cu alloys support a stepwise development [51], but the Cu occupation of matrix positions in the substituted planes of GP-I and GP-

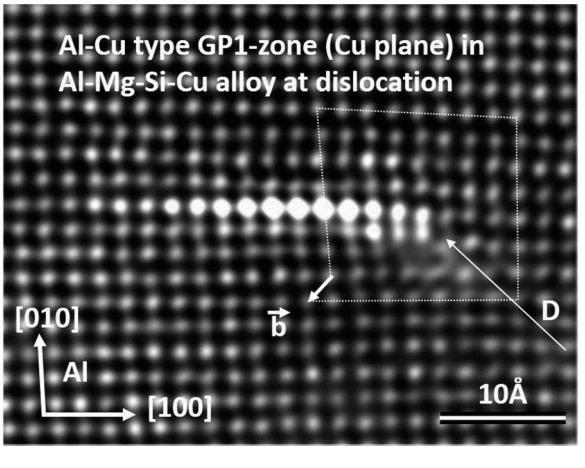

Figure 2. <001>Al projection of Al-Mg-Si-Cu alloy (aged 15 min at 200°C). Bright columns show a Cu-plane (GP-I zone) at a screw dislocation (D). *A* (dotted) loop reveals the burgers vector ($\vec{b}$).

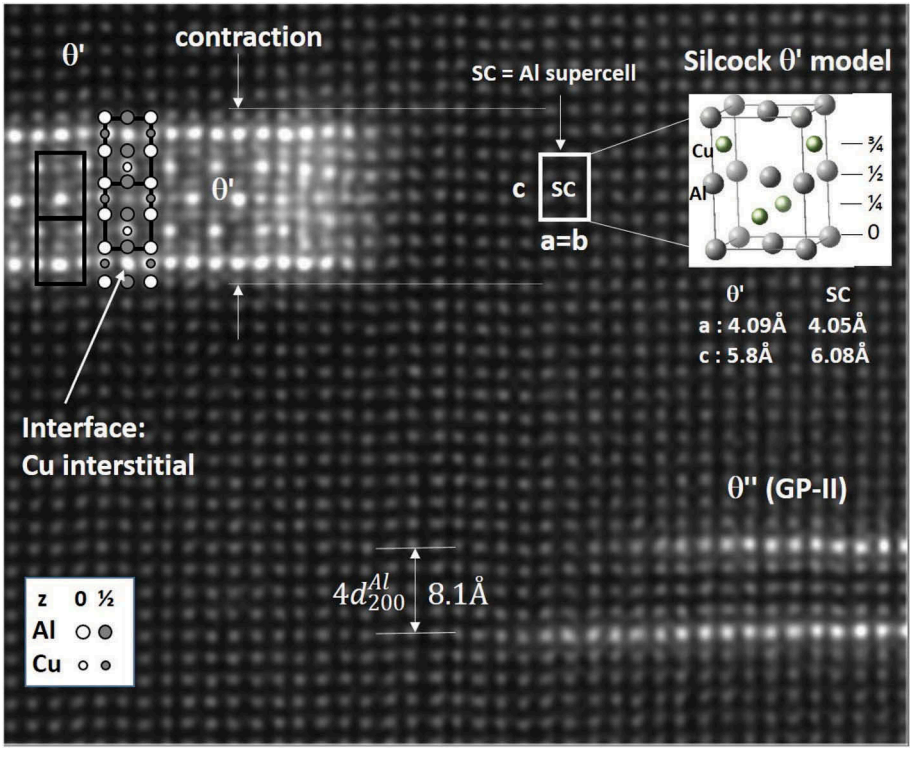

Figure 3. <001>Al projection of Al-5Cu alloy heat-treated 2 h at 185°C, showing θ'' (GP-II) zone and θ'. The two Cu planes of θ'' contain three {010}Al planes. Interface planes of θ' have only Cu, relating to (filled) interstitials. Each θ' cell has two vacancies relative to matrix, one per Cu-plane (at ¼ and ¾). θ' visibly contracts the lattice, as c is ~4.6% smaller than in the Al super cell.

II zones is still unclear [44]. The third step is the θ' phase, also a platelet with composition Al_2Cu [52]. Like for GP-II, Figure 3 shows that two Cu-planes define the d_{200}^{Al} interfaces, with seven planes between (five {010}Al planes). Relative to the Al lattice, the θ' cell spans two Al cells, but contains just six atoms, which means it contains two vacancies, relating to interstitials, seen in the insert in Figure 3, top right. They are 'missing' atoms in the one-forth and three-forth height, with respect to the Al lattice, which means that this phase consumes vacancies. The interstitials can be occupied, as is clear from the interface planes, of which both Al and θ' claim ownership. A transformation from GP-II to θ' requires replacement of two Al atoms by Cu and two more by vacancies. The θ' phase is therefore an ordering of solute and vacancies and shows both are building blocks of the precipitates. It has recently been shown that Cu makes use of the interstitials to form complex superstructures [53].

The equilibrium phase θ-Al_2Cu is alone on the Al-rich side of the equilibrium-phase diagram (Figure 1). It forms by slow cooling or heating

at higher temperature. Being incoherent, it contributes little to hardening. It is tetragonal (I4/mcm) with $a = b = 5.9875$ Å and $c = 4.807$ Å [54,55]. The structure differs significantly from θ' and is more densely packed. A variant is the orthorhombic Ω-Al_2Cu phase ($a = 4.96$ Å, $b = 8.56$ Å and $c = 8.48$ Å), only occurring with additions of silver [56–59], with Ag-free bulk structure. Coherence in the aluminium is described by the supercell $a = 6d^{Al}_{42\bar{2}} = 4.96$ Å, $b = 6\ d^{Al}_{02\bar{2}} = 8.59$ Å and $c \sim 4d^{Al}_{111} = 9.35$ Å. Growth occurs along the normal $[001]\Omega \parallel [111]$Al, i.e. with poor coherency. It is important because it shows how precipitation in alloy systems connects.

Atom probe studies conclude that the Ω-phase nucleates from a GP-zone in Al-Cu-Mg-Ag alloys, a platelet containing all solute elements on {111}Al planes. It is overlaid by a thicker plate of bulk composition Al_2Cu [58,59]. Figure 4(b) gives an example in an Al-3Cu-1Mg-0.5Ag (wt%) alloy, heated to maximum hardness (16 h ageing at 170°C after quench from (1 h) solution treatment at 440°C). A part of a larger Ω-particle shown in Figure 4(c) is of an alloy Al-4Zn-2Cu-1Mg-0.7Si after 1 h at 480°C, a quench and 32 days ageing at 150°C. Cu and Zn replace each other (and Al) in these structures. The interfaces between the particles and the Al matrix in Figure 4(b) and (c) are clearly similar, although overlap with the Al matrix

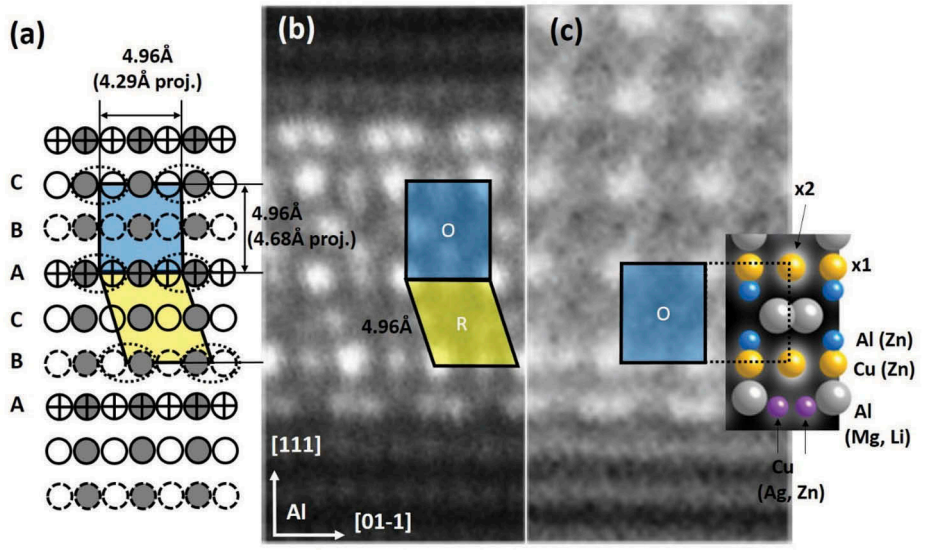

Figure 4. (a) Ω-Al_2Cu supercell in aluminium in [1-2-1] projection. (*b-c*) Two HAADF images of Ω-plates edge-on. In (a), dotted ovals show how (pairs of Cu) columns in Al can merge to yield the (high intensity) corners of the projected real cell. (Al occupy remaining positions.) Orthorhombic (O) and rhombohedral (R) cell are projections of same six-atom cell, relatively rotated. (b) A Ω-platelet structure, spanning 7 {111}Al planes in alloy Al-1Mg-3Cu-0.5Ag (wt%) and two relatively rotated layers (O, R). (c) Lower part of a Ω-precipitate. Corners have double occupation (×2). Right insert shows substitutions in various precipitate phases built by the same cell.

reduces the contrast of the image. However, the bulk structure is well known [58]. Figure 4(a) shows the actual building block, or the smallest asymmetrical unit of the supercell given above, along a < 211> Al direction. The letters A, B and C to the left of the figure refer to the three identical, Al planes of the face centered cubic (FCC) symmetry. The supercell in Al is defined by type < 211> lattice vectors, and smallest periodic distance 4.96 Å. With (111)Al as base plane, one set is $\{\frac{a_{Al}}{2}[1\bar{2}1], \frac{a_{Al}}{2}[11\bar{2}], \frac{a_{Al}}{2}[211]\}$, which defines a rhombohedron. The two shaded cells in Figure 4(a) are projections along two < 211> directions at 60° angle. (The second set related to the same (111) Al plane is obtained by rotating around [111]Al.) Thus, the platelet in (*b*) is formed by two layers of rhombohedra, relatively rotated 60°. The alternation of layers does not always happen, as is obvious from Figure 6(c). Here, in the normal Ω-phase, all layers take the same direction.

The Ω-phase can be explained as a displacive transformation from a matrix ordering of Cu, with short displacements and equal number of atoms. The supercell (Figure 4(a)) consists of six atoms. After ordering in the Al matrix (preceded by Ag ordering on a {111}Al plane), two and two Cu column segments should fuse, becoming the corner columns (pairs within dotted ellipses). The Cu atoms end up above each other in the < 211> viewing direction, with twice the Al occupancy, while the remaining four Al-atoms undergo smaller displacements. This procedure explains the bulk structure of the Ω-phase, composition and orientation. The interface layer is an ordering of Cu on the outer {111}Al-plane. Since the number of atoms over a coherent precipitate is conserved and Cu is smaller than Al, size difference explains contraction of the precipitate. No Ω-phase forms for high Mg/Cu ratio, even with Ag [60].

The same procedure explains the T1 phase in Al-Li-Cu alloys [61] and the η' and η-phases in the Al-Mg-Zn system [62], with slightly different dimensions. In Figure 4(c), the different atomic species are indicated for their typical positions in the supercell. In real precipitates, the single-occupancy Cu positions sometimes show weaker intensity than expected, which indicates Al incorporation. The intensity pattern is similar for all these phases concerning the {111}Al interface layer, and is shown in detail in Figure 5.

Although precipitates in Al-Mg-Zn are mainly plates with many orientation relations [63], needles are sometimes observed. Figure 6 is an example in a <2-1-1> Al projection in Al-8.5Zn-2.2Mg-1.9 Cu (wt%) [62]. The rhombohedral cell found in Ω-Al_2Cu, η'-$MgZn_2$ and the T1-phase is recognized. Two zinc atoms (×2) define a corner of a rhomb, while single Zn atoms divide the edges. The rhomb encloses two inner Mg atoms. In the orthorhombic projection, corners are the same, while we see internal pairs of Mg and Zn. Compare with Figure 4(c). The rhombohedra meet at the double Zn corners where they always form Zn-

centred icosahedra. In Figure 6, the 10 atoms defined by two pentagons (open/closed circles around a corner), plus 2 atoms on the corner yield the 12 vertices of the icosahedron. The remaining Zn atom on the cell corner axis defines the centre. In general, Cu partly occupies Zn-positions [62,64].

All corners appear with fivefold symmetry, but only occasionally local perfect fivefold axes exist. In Figure 6, the superposed pentagon indicates

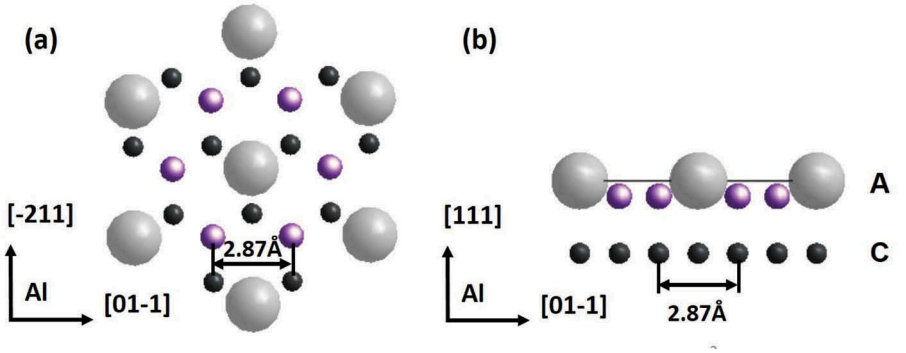

Figure 5. (a) The interface layer and the immediate Al (111) plane in [111] projection. Al atoms are coloured black. The interface layer is a 'split' Al layer, with 2/3 of positions occupied by a small atom (pink, medium-size atoms), like Cu or Zn (ideally 2.87 Å apart) and the remaining positions by a larger atom (Mg, Li, Al). (b) The same in [−211] projection. Compare with Figure 4.

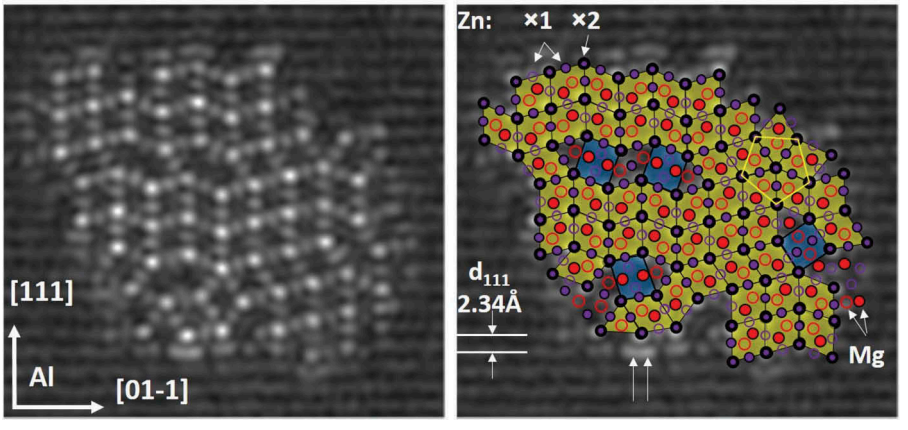

Figure 6. [1-2-1] Al projection in an alloy Al-8.5Zn-2.2Mg-1.9 Cu (wt.%), along a heavily faulted structure explainable by periodic stacking (in viewing direction) of columns of the same rhombohedral supercell building η and η' phase [62]. Local fivefold symmetry exists around all the doubly occupied (×2) cell corners. A pentagon shows five rhombohedra sharing a corner, forming a near-perfect pentagonal (icosahedral) symmetry. Lower arrows indicate interface Zn atoms split a {111}Al plane locally outside corners, like shown in Figure 5(b). Open/filled circles indicate different plane heights, while the doubly occupied corners have two special heights. Cu is intermixed with Zn.

Table 1. Precipitate phases in alloy systems Al-Mg-Si and Al-Mg-Cu.

Structure/~ideal composition	Space group	Unit cell parameters [Å]/[degrees]
Al	Fm3m	4.05
β-Mg_2Si [74]	Fm-3m	6.35
$U1$-$MgAl_2Si_2$ 'A' [75]	P-3m1	4.05, 6.74/120
β'' - $Mg_4(Al_xMg_{1-x})Si_4$ [29,76]	C2/m	15.16, 4.05, 6.74/105.3
U2-$Mg_4Al_4Si_4$ [77]	Pnma	6.75, 4.05, 7.94
β' -Mg_9Si_5 [79]	P63	7.15, 12.15/120
B' ~ $Mg_{48}Al_{16}Si_{36}$ [80,81]	P63/m	10.30, 20.25/120
C – $Mg_4AlSi_{3.3}Cu_{0.7}$ [82]	P21/m	10.33, 4.05, 8.10/101.3
Q – $Mg_9Al_3Si_7Cu_2$ [83]	P-6	10.30, 4.05/120
L~ $MgAl_{0.32}(Si_{1-x}Cu_x)$ [29]	–	1D periodic (c = 405)
GP-$Mg_4(Al_xMg_{1-x})Si_4$ [84]		1D periodic (c = 405)
GPB – $Mg_3Cu_3Al_2$ [84–87]	–	1D periodic (c = 405)
S' – $Mg_4Cu_4Al_8$ [88]	Cmcm	4.05, 9.27, 7.12

one. The lower arrow pair indicates the {111}Al interface plane is split compositionally, as shown in Figure 5. Open filled/circles belong to two different heights [62]. Similar rhombohedra are known to form non-periodic icosahedral quasicrystals [65–67]. A number of different orientations of the η'-phase can exist [63], reflecting the many ways the cell can be stacked. In this particle, most rhombohedra lay in the (01–1)Al plane rather than in the (111)Al plane (horizontal), which may prevent the plate shape.

Precipitates in Al-Mg-Cu and Al-Mg-Si alloys

Table 1 gives an overview of the most important precipitates occurring in the two systems. Diamond Si may also be considered as stable in Al-Mg-Si [68].

Al-Mg-Cu alloys are used in aircraft structures and for a range of other structural applications [6,7]. The precipitation sequence (Figure 1) takes two paths [26,69,70]:

$$\begin{aligned} &\text{SSSS} \rightarrow \text{solute clusters} \rightarrow \text{GP1} \rightarrow \text{GP2}(\text{q}'') \rightarrow \text{q}' \rightarrow \text{q} = \text{Al}_2\text{Cu}, \\ &\text{SSSS} \rightarrow \text{solute clusters} \rightarrow \text{GPB} \rightarrow (\text{S}'') \rightarrow \text{S}' \rightarrow \text{S} = \text{Al}_2\text{CuMg}. \end{aligned}$$

In Al-Mg-Si alloys the precipitation sequence is [71–73]:

$$\text{SSSS} \rightarrow \text{soluteclusters} \rightarrow \text{GP} \rightarrow \text{b}'' \rightarrow \text{b}' \rightarrow \text{b} = \text{Mg}_2\text{Si}.$$

The phases are listed in Table 1 [74–88]. β' [79] here also comprises $U1$ [75], $U2$ [77] and B' [79,80], also called A, B and C [73]. These precipitates can often be mixed [77,78].

Al-Mg-Si alloys are not as strong as most 2xxx and 7xxx alloys, but have good formability, corrosion resistance, surface qualities, welding and machining properties, which satisfy a range of structural purposes. For both Al-Mg-Si and Al-Mg-Cu, the precipitates giving strength are needles, rods or laths, along <100> Al.

GP-zones and the β″-phase in Al-Mg-Si. Structures based on 1D defects

The needle-shaped β''-phase is the most important hardening precipitate in the AA6xxx system. The structure was determined by electron diffraction as two units of Mg_5Si_6 [76]. The monoclinic (C2/m) cell refined to parameters a = 15.16 Å, b = 4.05 Å, c = 6.74 Å and β = 105.3°, a cell first reported by Edwards et al. [72]. The unique b-axis is along the needle axis in a <100> Al direction. Calculations later found it to contain aluminium [89,90], as confirmed by recent atomic resolution mapping by energy dispersive x-ray spectroscopy [91]. A more precise bulk composition is therefore $Mg_{4+x}Al_{3-x}Si_4$, ($x \in [0, 1]$), near the Mg/Si ratio found by atom probe field ion microscopy [72,92]. The variant in Figure 7 has bases $a||[320]$ and $c||[1\bar{3}0]$ in the (001) Al plane, and $\boldsymbol{b}$ along [001] Al, which depend on size and composition, as calculations indicate [90]. A supercell in Al matrix is:

$$a_{\beta''} = 13d^{Al}_{3\bar{2}0}(14.60\text{Å}), b_{\beta''} = d^{Al}_{001}(4.05\text{Å}) \text{ and } c_{\beta''} = 5d^{Al}_{130}(6.40\text{Å}).$$

Figure 7 shows the β'' particle as a very thin needle, with cross-section consisting of few molecular units called 'β''-eyes'. An 'eye' is a projected 1D string of molecules, corresponding to Al FCC cells with Mg as corners, Si at the four lateral face centres, an Mg or Al atom at the cube centre, and two outer Al atoms (left/right sides). See detailed sketch in Figure 8. The Al outliers are preferred sites for other atoms, such as Cu [29,93]. A '+' indicates that the top/bottom face atom jumps to the FCC cube centre (i.e. an interstitial position) towards a vacancy, which gets locked [94]. The vacancy is required in the front to avoid too close atoms. The resulting

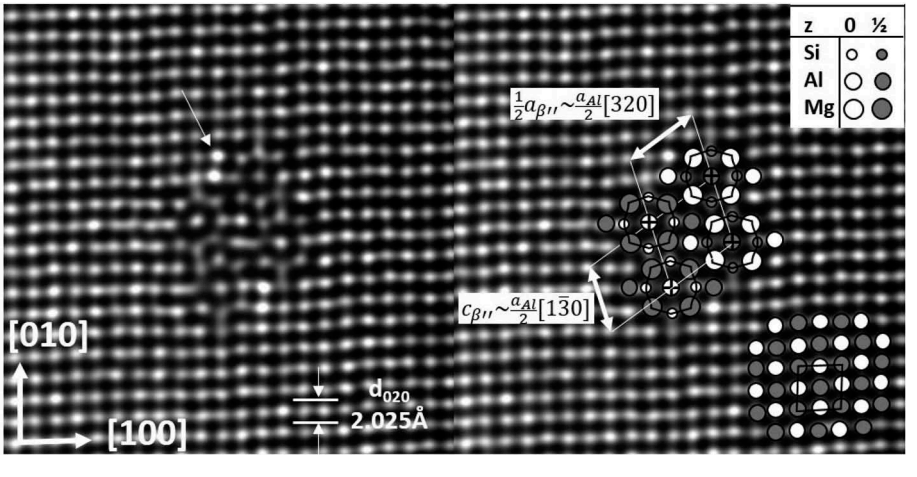

Figure 7. Cross-section of a small β'' precipitate in Al-1.2Si-0.3Mg-0.04Cu, aged 30 mins at 185°C. Four eye-like molecules span a semi-cell. The monoclinic b-axis is parallel with the viewing <001> Al direction. A molecule is comparable with one Al cell (see Figure 8). High intensity columns indicate Cu (also seen at the lower β'' interface).

centre column is a 1D defect and a vacancy trap [94]. Calculations show this column can consist of Mg or Al atoms [89,90], as well as experiments [90,91]. The arrow in Figure 7(a) points to columns of higher intensity (atomic number), here interpreted as Cu.

Figure 8 shows two magnifications of an image of with two β''-eyes in the Al-matrix, arranged as the upper part of the β'' phase in Figure 7. Isolated 1D strings in both Al-Mg-Si and in Al-Mg-Cu alloys have been detected by HAADF [84,85]. Because of higher STEM contrast of Cu atoms, they are only demonstrated in Figure 9 in an Al-Mg-Cu alloy. The arrows point out two molecules. Referring to Figure 8(d) and the calculations in Table 2, here Cu takes the place of Si. They relate to the Guinier-Preston-Bagaryatsky (GPB) zones in Al-Mg-Cu determined by Kovarik et al., using HAADF and *ab initio* calculations [86,87]. Recently, they were shown to be explainable by connected pairs of isostructural molecules (eyes) as in β'' but with (different) separation $5d_{210}^{Al}$ [29], i.e. 1D defect pairs [29].

The precipitates shown in Figure 9 fit the definition of GP-zones in Al-Mg-Si and Al-Mg-Cu [84]. The calculations in Table 2 assuming infinite long columns support the observations, demonstrating low energy for six compositions. Having the central column interstitial strongly reduces

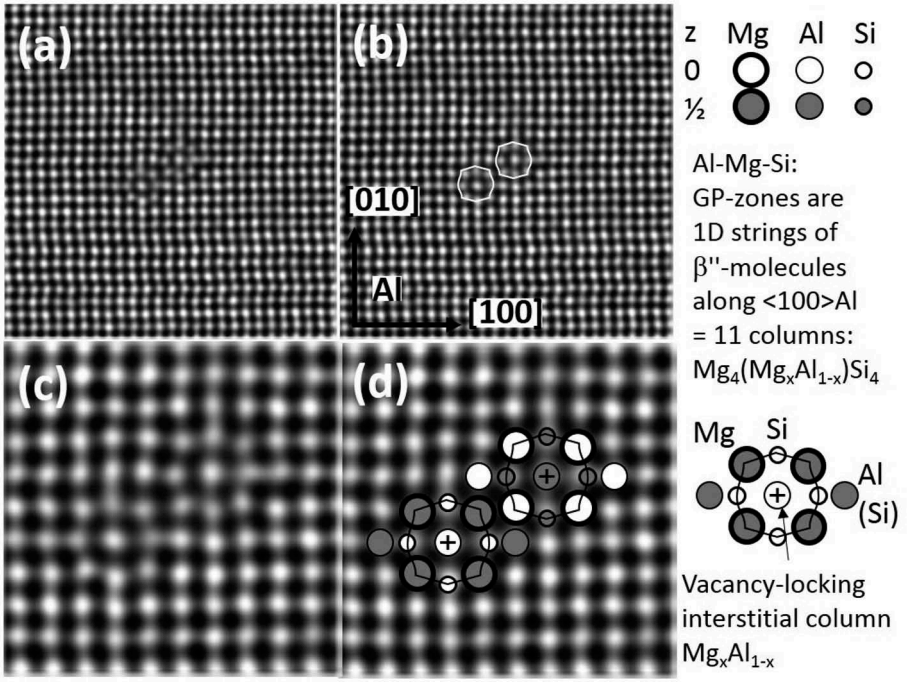

Figure 8. <001>Al zone with two β'' eyes in projection. (Same alloy as in Figure 7, but aged 30 days at 90°C). (b) is (a) with overlay. (c) and (d) show higher magnification. Single eyes are not shown. The two eyes connect along a < 320> Al direction, as for β'' (Figure 7), by triangularly arranged Si columns (Si-network). Table 2 shows that Mg in the centre slightly lowers energy.

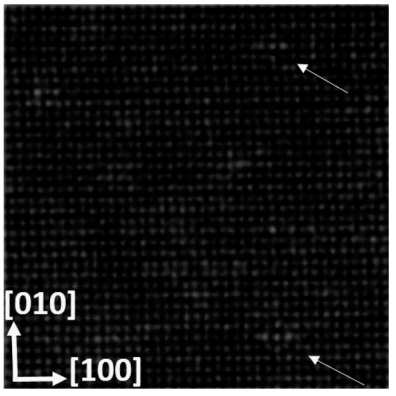

Figure 9. HAADF image of an Al-3 Mg-1 Cu alloy (wt%) [60], heat-treated 1 min at 170°C. Arrows point out two independent 1D GP-zones consisting of four columns each of Cu and Mg, isostructural to the 1D zones in Al-Mg-Si as shown in Figure 8, with Si replaced by Cu. Calculations in (Table 2) indicate Al centre and ratio Mg/Cu = 1.

energy. The most stable configurations are Mg_4Si_4Mg and Mg_4Cu_4Al with interstitial Mg and Al columns, respectively. Needles without interstitial defects are also possible, indicating they represent initial arrangements, which capture a vacancy allowing the central column to shift. While Si columns in one eye form a square, Figure 8(d) shows that the ones between eyes arrange as rhombs/triangles. Figure 7 demonstrates that the Si-columns between eyes arrange hexagonally. In fact, the common network of the

Table 2. DFT calculations showing stability for 12 (infinitely long) GP-zones without/with the interstitial 1D defect, by formation enthalpy (energy change) for 64-atom supercell (4 × 4 × 1 Al cells) and per solute. This means 8 or 9 solute columns per 64 infinite columns. The molecular embedded string is Mg_4A_4B, where *A* is Si or Cu, and *B* is the centre atom (Al, Mg, Cu). '*D*' in cell composition says the centre column is interstitial (a defect). The solute replaced columns Mg_4Cu_4 around an interstitial Al column ($Al_{56}Mg_4Cu_4D$) yield the most stable GP-zone. Without the defect, $Al_{56}Mg_4Cu_4$ ranges second worst. Note that Cu can be in the centre, as has recently been observed for β'' [95].

Molecule Mg_4A_4B	Calculation cell composition	Formation enthalpy (eV) per cell/per solute	
Mg_4Cu_4Cu	$Al_{55}Mg_4Cu_5$	−0.088	−0.01
Mg_4Cu_4Al	$Al_{56}Mg_4Cu_4$	−0.168	−0.021
Mg_4Cu_4Mg	$Al_{55}Mg_5Cu_4$	−0.308	−0.034
Mg_4Si_4Cu	$Al_{55}Mg_4Si_4Cu$	−0.403	−0.045
Mg_4Si_4Al	$Al_{56}Mg_4Si_4$	−0.422	−0.053
Mg_4Si_4Mg	$Al_{55}Mg_5Si_4$	−0.720	−0.080
Mg_4Si_4Al	$Al_{56}Mg_4Si_4D$	−1.233	−0.154
Mg_4Cu_4Cu	$Al_{55}Mg_4Cu_5D$	−1.352	−0.150
Mg_4Si_4Cu	$Al_{55}Mg_4Si_4CuD$	−1.360	−0.151
Mg_4Si_4Mg	$Al_{55}Mg_5Si_4D$	−1.411	−0.157
Mg_4Cu_4Mg	$Al_{55}Mg_5Cu_4D$	−1.459	−0.162
Mg_4Cu_4Al	$Al_{56}Mg_4Cu_4D$	−1.769	−0.221

precipitates reflects that Si atoms form connected square-based pyramids, with bases on the (100) Al plane [84,85]. In β'', they are edge-connected. This suggests how transformation from a GP-zone to β'' takes place: Si gradually fills the matrix columns outside the particle ideal for making pyramids, extending the Si network (see below). It may mean a lower particle Mg/Si ratio exists during growth than the bulk value shows, supporting the Mg_5Si_6 measurements [76].

Precipitates, column rules and nearest neighbour numbers

In precipitates in Al-Mg-Si and Al-Mg-Cu, columns identified with larger Mg atoms generally are surrounded by five columns for both planes, columns of Si and Cu atoms show a threefold surrounding, while aluminium has fourfold column surrounding [29]. Exceptions exist only for the less coherent precipitates (β, β' and U1), although the same rules apply in the interface. The reason can be found with the β'' molecule (GP-zone) in Figures 7 and 8. When (a segment of) the <001>Al centre column shifts d^{Al}_{002} to the next plane (atoms move to interstitial positions), four surrounding columns obtain fivefold surroundings (15NNs) and four others threefold (9NNs). Since larger atoms (Mg) prefer high NN numbers and smaller atoms (Si, Cu) lower, this decomposition of Al reduces strain. The resulting symmetry gives the observed single β''-eye or GP-zone, each eye locking one vacancy.

In Figure 10, we show the structure of the S′ phase interpreted by the column rules. The main boundary of S′ is the *a*-*b* plane parallel with a {210} Al plane. S′ is orthorhombic with space group Cmcm (No. 63). The stable version has parameters a = 4.0119 Å, b = 9.265 Å and c = 7.124 Å [88,96,97]. The image shows the b-parameter nearly equals $a_{Al}[2\bar{1}0]$, i.e. $10d^{Al}_{4\bar{2}0}$ = 9.06 Å. The ideal parameter is 2.3% larger, which could mean expansive strain along $b_{S'}$. As the particle grows, the contribution to energy from the interface loses significance, and the structure becomes less dependent on the Al matrix. The column rules originate with the Al matrix, and should apply best for the smallest metastable phases.

Precipitates in the Al-Mg-Si-Cu system and the Si-network

With Cu in the alloys, the Al-Mg-Si precipitation sequence changes considerably. With increased amount of Cu, *U*1, *U*2 and *B*′ disappears, as well as β' and β''. In Mg-richer alloys with Cu, the β'' phase is replaced by the disordered *L*-phase [23]. The precipitation sequence has been reported as [98–102]:

$$\text{SSSS} \rightarrow \text{soluteclusters} \rightarrow \text{GP} \rightarrow \beta'', \text{L}, \text{S}, \text{C}, \text{QP}, \text{QC} \rightarrow \beta', \text{Q}' \rightarrow \text{Q}(\beta)$$

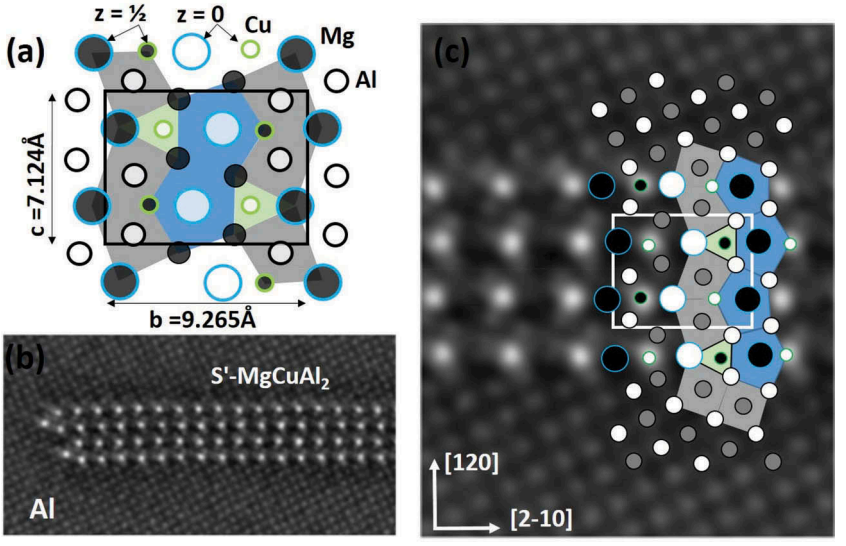

Figure 10. (a) Structure of S′-$MgCuAl_2$ phase along *a*-axis (*a* = 4.05 Å) illustrates column rules. Large to small disks are Mg, Al and Cu. Polygons show five-, four- and and threefold surrounding column symmetry. The two heights in the viewing direction (white and dark fill) align with Al-planes (z = 0, ½). (b) HAADF of <001>Al projection of Al-3Cu-1Mg (wt%) heat-treated 11 days at 170°C, with Al-embedded *S′* plate along its coherent *a*-axis. (c) Detail of particle in (*b*) partly superposed, showing consistent column arrangement/symmetry around columns across the particle. The same applies to all coherent precipitates in Al-Mg-Si and Al-Mg-Cu system. The interface is a 'fence' of alternating Mg and Cu columns.

These coherent phases follow the set of column rules discussed above [29]. However, for the ideal structures of all the precipitates of the Al-Mg-Si alloys based on solute Mg and Si (and Cu), an additional condition applies. Viewed along the main extension of the precipitates (<100>Al), three neighbour Si-columns form a triangle with ~4 Å edge, i.e. a hexagonal arrangement around another column. These triangles join and build the 'Si-network' [103,104]. Since the columns refer to the two different planes (heights), the Si sub-lattice itself is usually not truly hexagonal. The precipitate structures can all be explained as built on this network.

If columns between form no particular arrangement, in projection, a basic hexagonal cell $a \sim 4.0$ Å, $c = 4.05$ Å appears [103–105]. This is the phase reported as QP [100–102,105]. The network geometry had been investigated by Cayron et.al. and called 'QP-lattice' [102,105], but not linked to columns of Si as precipitate structures were unknown and the high-resolution HAADF-STEM techniques were unavailable. It was explained by 'sub-unit triangular clusters' and used for building average models of β' ($c = 4.05$ Å) and the QC phase. The *L*-phase is lath or plate-like. It is disordered on an ordered Si-net, but still follows the column rules [29,101,104]. It is probably what was described as a type on the QP lattice

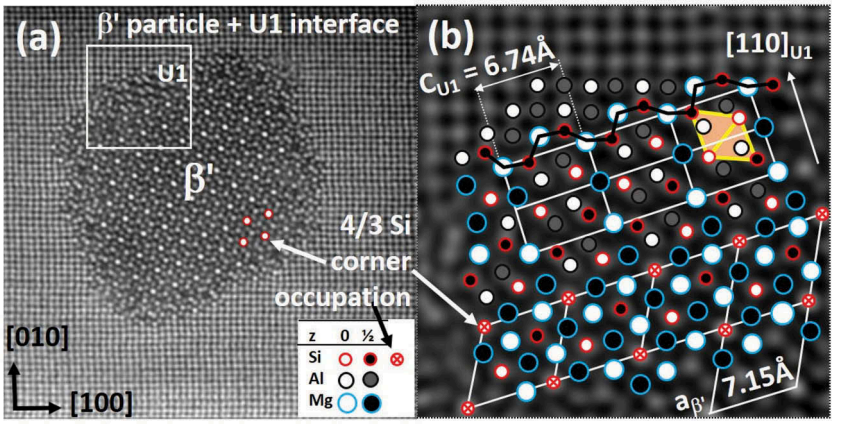

Figure 11. Alloy Al-0.7Mg-0.35Si-0.1Co (at%) aged 67 h at 200°C. (a) A *β′* rod demonstrates the Si network with increased intensity for corners (4 Si atoms per 3 in other columns). (b) Overlaid region with *β′* interface along <310>Al direction. *U*1 interphase bridges *β′* to the matrix and ends it with the normal Mg-Si alternating column interface. Column rules apply only in the interface of these less coherent phases. In the upper right unit cell of *U*1, the rhomb signifies a projected octahedron (two pyramids base-to-base) – the basic unit in the Si-network, Mg_2Si and diamond Si.

[102,105] and called 'QP2′ in a recent work [106]. It is a hardening phase, but more temperature resilient than *β″* [23]. The S-phase (not to be confused with S′ in Al-Mg-Cu, see Figure 10) is a disordered Cu-containing *β′*-variant on the network with normal orientation [101]. QC – a simpler, *β′*-variant which is common with Ag [107] – can also form with Cu [105], and the (6.7–7 Å) hexagonal basis is smaller than for ordinary *β′* [79]. *C* is a plate-like Cu-containing monoclinic structure, often with inhomogeneous distribution [82,101]. The *Q′*-phase appears with over-ageing. It is considered isostructural with the equilibrium phase *Q*-$Mg_9Al_3Si_7Cu_2$ [38,83].

In the network, a column between Si columns is never Si. However, Cu can replace Si. This is the reason in Table 1, that the Si (+ Cu) content in the precipitates roughly amounts to one-third. In *β′*-$Mg_{18}Si_{10}$, an extra Si atom per three cells gives a slightly higher content (0.36). The higher occupancy in the corner is clear from Figure 11(a). In Figure 11(b), the overlay identifies the network and shows that the (upper) interface consists of a layer of the hexagonal *U*1-$MgAl_2Si_2$ phase (a = 4.05 Å and c = 6.74 Å). It is interesting because of a high Si/Mg ratio and a growth direction normal to its hexagonal axis, giving a slightly deformed Si network relative to the matrix by columns along <100>*U*1 [75]. Figure 11 shows that the column rules only apply in the outer interface, i.e. about the columns forming the usual Mg-Si column band (indicated by a black wavy line). The *U*1 and *β′* phases depend less on the matrix. The conserved column symmetry of the outer interface structure suggests that the lateral growth

takes place via the same decomposition mechanism as described above. The indicated rhomb in the upper, right *U*1-cell defines the projected unit of the Si-network. In 3D, it is a Si octahedron (two square-based pyramids put together base-to-base) [84,85]. The octahedron exists in the equilibrium-phase β-Mg_2Si as well as in diamond silicon. This indicates that the Si network is a preliminary construction with the goal to form the low-energy phases diamond Si and/or Mg_2Si, when limited to the Al matrix. It can be shown that every Si atom in all Al-Mg-Si precipitate structures is a vertex of such Si pyramid.

The network exists also in β'', as recently demonstrated in reference 29. Cu, Ge, Zn and Ag have been observed to substitute Si. Ge generally makes β'' disordered. It stabilizes hexagonal network β' fragments [108–110] and changes the stacking of the β'' units, producing new variants of β''-phases [24]. A recent paper discusses effects of incorporation of impurity elements in β'' [85].

Fragments of β'', *U*2 and β' are frequently found in the same needle [29,77,105]. Figure 12 is an example of disorder [78] with square GP-units. Assuming unmixed columns, Figure 12 yields a composition $Mg_{72}Si_{71}Al_{43}X_{15}$, where '*X*' signifies number of missing columns relative to the aluminium. The column rules and Si-network suffice to explain this very disordered structure. The outer 'fence' of alternating columns of small and big atoms, with surrounded five- and threefold symmetry, even for disordered and partly incoherent phases (Figures 10 and 11) directly point to the defect decomposition mechanism operating at the interface.

Conclusions and perspectives

We have reviewed structures of the essential metastable precipitates for hardening in four important commercial aluminium alloy systems; Al-Cu, Al-Mg-Cu, Al-Mg-Zn and Al-Mg-Si and demonstrated how they relate via simple orderings and supercells in the Al matrix. Some new results are included, by high-angle annular dark-field electron microscopy and density functional theory calculations.

A rhombohedral unit – is a cage of four Zn and two Mg atoms is the basis of the plate-like η' and η-$MgZn_2$ phases in Al-Mg-Zn alloys forming on {111}Al planes, and explains even disordered needles in the alloys. Isostructural units exist for the Ω-Cu_2Al phase in the Al-Cu-(Mg) system with Cu replacing Zn, as well as for the T1 phase in the Al-Li-Cu. The rhombohedral unit is essentially a supercell in the Al lattice spanned by three vectors along <211>Al directions. Challenges in these systems include understanding the rhombohedral unit better, why it is preferred over single Cu-planes in Al-Cu and Al-Cu-Mg, details of its formation, stability, its flexibility regarding various elements, how units are added and how it connects to quasicrystals.

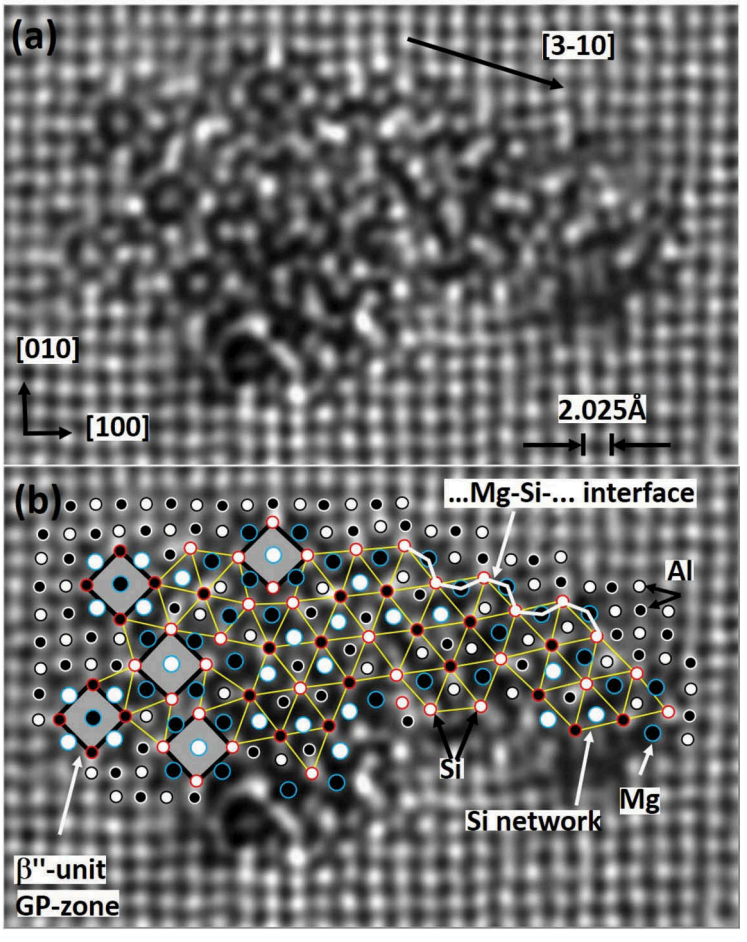

Figure 12. (a) Cross-section of disordered precipitate needle in a commercial 6060 alloy, aged 5 h at 190°C. (b) With suggested overlay. Upper part shows partly coherence along <310>Al. Grey squares are individual β'' molecules (GP-zones). The (projected) Si-network is indicated by yellow lines. Atoms/heights may be inferred by network (Si-columns), spacing, intensity and a consistent column symmetry (Mg: fivefold, Si: threefold and Al: fourfold). The interface reflects that of a general coherent precipitate in Al-Mg-Si; i.e. a surrounding wall of alternating Mg and Si columns along the needle <100>Al direction. Open/filled symbols reflect the two {100}Al plane heights.

The early stages in Al-Mg-Si and Al-Mg-Cu systems have isostructural GP-zones being 1D strings along <100>Al, identical to the eye-like units of the β''-phase, where Cu can replace Si.

Calculations show GP-zones can take different compositions, the most stable being Mg_4Si_4Mg and Mg_4Cu_4Al, with Mg and Al as central interstitial columns. Solute clusters for the GP-zones are likely short defect-free needles using a vacancy to produce a central interstitial column. The interstitial column splits the surrounding matrix in columns of different NNs, effectively explaining the solute distribution in GP-zones. Each 1D

string traps one vacancy. The defect describes a new decomposition mechanism, which needs to be investigated. The vacancy trapping means the numbers depends on the amount of quenched-in vacancies in the alloy. To each trapped vacancy corresponds one interstitial defect. The defect is the real source of strain in a β'' precipitate and in a GP-zone. Challenges involve understanding lateral growth of β'', and how material strength relates to such defects, and whether ways to increase their numbers. For example, how is the number of defects limited by quenched-in vacancies? It relates also to the Al-Mg-Zn alloys, as no vacancies are locked in the basic units, which could be behind the greater amount of useable solute in these alloys.

In all metastable precipitates of these two systems, Mg, Al and Si/Cu define columns along the main <100>Al precipitate extension with five-, four- and threefold column symmetries, even in disordered precipitates. All are explained by the same mechanism. Less coherent phases with bulk structures not following the column rules are surrounded by a wall of alternating Mg-Si- or Mg-Cu-replaced <100>Al columns, which do obey the rules. It indicates this is also the mechanism for lateral growth. It offers a new way to investigate growth and dissolution in these systems.

The Si-network in the Al-Mg-Si system is explained in terms of square-based Si-pyramids forming in the matrix, which join either base-to-base (octahedrons) as in diamond silicon, $U1$-$MgAl_2Si_2$ and β-Mg_2Si, or edge-to-edge as in β'' and most other phases. Thus, the Si-network is specific for this system. The tendency of silicon to form pyramids or octahedrons in the Al matrix determines the Si network positions relative to the Al lattice. i.e. in precipitates in the Al-Mg-Si system, the tendency to form another pyramid influences the next column that will become an interstitial defect column. In Al-Mg-Cu, there is no similar tendency; thus, only the column rules are observed. The network is undisputable. How it forms can now be investigated in terms of the pyramids. In β' and B′, the network is special, as more Si exists in the 00z columns. A challenge is to understand how Si pyramids are distributed in these phases.The hardest challenge is probably to get a proper understanding of the very early stages, ordering of solid solution and how it leads to precipitation [84].

Acknowledgments

We acknowledge Hydro Aluminium and the Research Council of Norway (RCN) for support through the BIA 'RolEx' (Grant 219371), the FRINATEK project 'Fundamental investigations of precipitation in the solid state with focus on Al-based alloys' (Grant 221714), and the Hydro Fond project 121 at SINTEF. We acknowledge Dr Olaf Engler,

Hydro Al Rolled Products, Bonn for direct financial support. We acknowledge Drs. Williams Lefebvre from CNRS/University of Rouen and Alexis Deschamps from SIMAP-INP Grenoble for previous support contributing to the 7xxx results study. The research was supported by the project NORTEM (Grant 197405) within the programme 'Infrastructure of the RCN'. NORTEM was co-funded by the RCN and the project partners NTNU, UiO and SINTEF. Computational resources were provided by NOTUR, c.f. http://www.sigma2.no (Grant NN8058K).

Disclosure statement

No potential conflict of interest was reported by the authors.

Funding

We acknowledge Hydro Aluminium and the Research Council of Norway (RCN) for support through previous projects, such as the BIA 'RolEx' (Grant 219371) and the 'FRINATEK' project 'Fundamental investigations of precipitation in the solid state with focus on Al-based alloys' (Grant 221714). We acknowledge SINTEF for the financing through the ('Hydrofond') project 'Understanding and multi-scale modelling of early stage precipitation in age hardenable Al-Mg-Si alloys" . We acknowledge Dr Olaf Engler, Hydro Al Rolled Products, Bonn for discussions and financial support. The research was supported by the project NORTEM within the programme 'Infrastructure of the RCN' (Grant 197405). NORTEM was co-funded by the RCN and the project partners NTNU, UiO and SINTEF. Computational resources were provided by NOTUR, c.f. http://www.sigma2.no (Grant NN8058K).

References

[1] J. Emsley, *The Elements*, 2nd, Clarendon Press, Oxford, 1991.
[2] The International Aluminium Institute http://www.world-aluminium.org/statistics/
[3] A. Wilm, Metall. Z. Ges. Hüttenkunde. 8 (1911) p. 225.
[4] M. Knauer, *Hundert Jahre Aluminiumindustrie in Deutschland (1886–1986): Die Geschichte Einer Dynamischen Branche*, Walter de Gruyter GmbH & Co, Berlin, 2014.
[5] F.W. Gayle and M. Goodway, Science 266(issue 5187) (1994) p. 1015. doi:10.1126/science.266.5187.1015.
[6] J.R. Davis, *Aluminum and Aluminum Alloys. ASM Speciality Handbook*, ASM International, Materials Park, OH, USA, 1993.
[7] P. Rambabu, N. Eswara Prasad, V.V. Kutumbarao and R.J.H. Wanhill, *Aerospace Materials and Material Technologies*, Indian Institute of Metals Series 1, 2017, p. 29. Springer Science+Business Media Singapore, 2017.
[8] Wikimedia commons. https://commons.wikimedia.org/wiki/File:Al-Cu-phase-diagram-partial-greek.svg
[9] J.B. Friauf and J. Amer, Chem. Soc. 49 (1927) p. 3107. doi:10.1021/ja01411a017.
[10] A. Meetsma, J.L. De Boer, S. Van Smaalen and J. Sol, State Chem. 83 (1989) p. 370. doi:10.1016/0022-4596(89)90188-6.
[11] K. Carling, G. Wahnström, T.R. Mattsson, A.E. Mattsson, N. Sandberg and G. Grimvall, Phys. Rev. Lett. 85 (2000) p. 3862. doi:10.1103/PhysRevLett.85.3862.

[12] J. Banhart, C.S.R. Chang, Z. Liang, N. Wanderka, M.D.H. Lay and A.J. Hill, Adv. Eng. Mater. 12 (2010) p. 559. doi:10.1002/adem.201000041.
[13] K. Mizuno, H. Okamoto, E. Hashimoto and T. Kino, Trans. Mat. Res. Soc. Jpn. 41 (2016) p. 243. doi:10.14723/tmrsj.41.243.
[14] P.B. Hirsch, J. Silcox, R.E. Smallman and K.H. Westmacott, Phil. Mag. 3 (1958) p. 897. doi:10.1080/14786435808237028.
[15] S. Yoshida, Y. Shimomura and M. Kiritani:, J. Phys. Soc. Jpn. 17 (1962) p. 1196. doi:10.1143/JPSJ.17.1196.
[16] V. Gavini, K. Bhattacharya and M. Ortiz, Phys. Rev. B 76. (2007) p. 180101. doi:10.1103/PhysRevB.76.180101.
[17] E.A. Mørtsell, C.D. Marioara, S.J. Andersen, J. Røyset, O. Reiso and R. Holmestad, Metall. Mater. Trans. A. 46 (2015) p. 4369. doi:10.1007/s11661-015-3039-5.
[18] M. Kubota, J.F. Nie and B.C. Muddle, Mater. Trans. 45 (2012) p. 3256. doi:10.2320/matertrans.45.3256.
[19] C. Wolverton, Acta Mater. 55 (2007) p. 5867. doi:10.1016/j.actamat.2007.06.039.
[20] D. Simonovic and M.H.F. Sluiter, Phys. Rev. B. 79 (2009) p. 054303. doi:10.1103/PhysRevB.79.054304.
[21] D. Mitlin, V. Radmilovic and J.W. Morris, Jr. Metall. Mater. Trans. A. 31 (2000) p. 2697. doi:10.1007/BF02830329.
[22] D. Mitlin, V. Radmilovic, U. Dahmen and J.W. Morris Jr., Metall. Mater. Trans. A. 32 (2001) p. 197. doi:10.1007/s11661-998-0335-3.
[23] C.D. Marioara, S.J. Andersen, J. Røyset, O. Reiso, S. Gulbrandsen-Dahl, T.E. Nicolaisen, I.E. Opheim, J.F. Helgaker and R. Holmestad:, Metall. Mater. Trans. A. 45 (2014) p. 2938. doi:10.1007/s11661-014-2250-0.
[24] E.A. Mørtsell, S.J. Andersen, J. Friis, C.D. Marioara and R. Holmestad, Phil. Mag. 97 (2017) p. 851. doi:10.1080/14786435.2017.1281461.
[25] G.D. Preston, Nature. 142 (1938) p. 570. doi:10.1038/142570a0.
[26] Y.A. Bagaryatsky, Dokl. Akad. Nauk SSSR. 87 (1952) p. 397 & 559.
[27] J.M. Silcock, J. Inst. Met. 89 (1960-61) p. 203.
[28] L. Kovarik, S.A. Court, H.L. Fraser and M.J. Mills, Acta Mater. 56 (2008) p. 4804. doi:10.1016/j.actamat.2008.05.042.
[29] S.J. Andersen, C.D. Marioara, J. Friis, R. Bjørge, Q. Du and I.G. Ringdalen, Mater. Sci. For. 877 (2017) p. 461.
[30] C.A. Geiger (ed.), *EMU Notes in Mineralogy*, 3 2001, p. 3. Eötvös Lórand University Press, Budapest, 2001.
[31] Ø. Ryen, O. Nijs, E. Sjölander, B. Holmedal, H.E. Ekström and E. Nes, Met. Mater. Trans. A. 37 (2006) p. 1999. doi:10.1007/s11661-006-0142-7.
[32] L. Vegard, Z. Physik. 5 (1921) p. 17. doi:10.1007/BF01349680.
[33] V.A. Lubarda, Mechanics of Materials. 35 (2003) p. 53.
[34] T. Sato, Y. Kojima and T. Takahashi, Metall. Trans A 13 (1982) p.1373.
[35] H. Zhou, W. Yao, C. Du, S. Song and R. Wu, Int. J. Electrochem. Sci. 12 (2017) p. 9542. doi:10.20964/2017.10.32.
[36] W.R. Osório, L.C. Noé Cheung and A.G. Peixoto, Int. J. Electrochem. Sci. 4 (2009) p. 820.
[37] D. Giofré, T. Junge, W.A. Curtin and M. Ceriotti, Acta Mater. 140 (2017) p. 240. doi:10.1016/j.actamat.2017.08.017.
[38] C. Wolverton, Acta Mater. 49 (2001) p. 3126. doi:10.1016/S1359-6454(01)00229-4.
[39] C. Wolverton and V. Ozoliņš, Phys. Rev. B. 73 (2006) p. 144104. doi:10.1103/RevB.73.144104.
[40] G. Kresse and J. Hafner, Phys. Rev. B. 47 (1993) p. 558.
[41] G. Kresse and J. Furthmüller, Comput. Mater. Sci. 6 (1996) p.15.

[42] P. Hohenberg and W. Kohn, Phys. Rev. B. 136 (1964) p. 864. doi:10.1103/PhysRev.136.B864.
[43] W. Kohn and L.J. Sham, Phys. Rev. A. 140 (1965) p. 1133. doi:10.1103/PhysRev.140.A1133.
[44] A. Biswas, D.J. Siegel, C. Wolverton and D.N. Seidman, Acta Mater. 59 (2011) p. 6187. doi:10.1016/j.actamat.2011.06.036.
[45] M. Karlík and B. Jouffre, Acta Mater. 45 (1997) p. 3251. doi:10.1016/S1359-6454(97)00003-7.
[46] T. Sato and A. Kamio, Mater. Sci. Eng. A. 146 (1991) p. 161. doi:10.1016/0921-5093(91)90275-R.
[47] V. Gerold, Scr. Metall. 22 (1988) p. 927. doi:10.1016/S0036-9748(88)80077-2.
[48] T.J. Konno, K. Hiraga and M. Kawasaki, Scr Mater. 44 (2001) p. 2303. doi:10.1016/S1359-6462(01)00909-5.
[49] K. Hono, T. Sakurai and H.W. Pickering, Met. Trans A. 20 (1989) p. 1585. doi:10.1007/BF02663192.
[50] L. Bourgeois, C. Dwyer, M. Weyland, J.-F. Nie and B.C. Muddle, Acta Mater. 59 (2011) p. 7043. doi:10.1016/j.actamat.2011.07.059.
[51] K. Joshi and S. Chaudhuri, Modelling Simul. Mater. Sci. Eng.. 24 (2016) p. 075012. doi:10.1088/0965-0393/24/7/075012.
[52] J.M. Silcock, Acta Cryst. 9 (1956) p. 680. doi:10.1107/S0365110X56001820.
[53] S. Wenner, J. Friis, C.D. Marioara, S.J. Andersen and R. Holmestad, Phil. Mag. 95 (2015) p. 3524. doi:10.1080/14786435.2015.1090639.
[54] J.B. Friauf and J. Amer, Chem. Soc. 49 (1927) p. 3107. doi:10.1021/ja01411a017.
[55] A. Meetsma, J.L. De Boer, S. Van Smaalen and J. Sol, State. Chem. 83 (1989) p. 370. doi:10.1016/0022-4596(89)90188-6.
[56] J.H. Auld, J.T. Vietz and I. Polmear, Nature. 209 (1966) p. 703. doi:10.1038/209703a0.
[57] K. Knowles and W. Stobbs, Acta Crystallogr. B. 44 (1988) p. 207. doi:10.1107/S0108768187012308.
[58] S.J. Kang, Y.-W. Kim, M. Kim and J.-M. Zuo, Acta Mater. 81 (2014) p. 501. doi:10.1016/j.actamat.2014.07.074.
[59] S.J. Kang, T.-H. Kim, C.-W. Yang, J.I. Lee, E.S. Park, T.W. Noh and M. Kim, Scripta Mater. 109 (2015) p. 68. doi:10.1016/j.scriptamat.2015.07.020.
[60] M. Mihara, C.D. Marioara, S.J. Andersen, R. Holmestad, E. Kobayashi and T. Sato, Mat.Sci. Eng. A. 658 (2016) p. 91. doi:10.1016/j.msea.2016.01.087.
[61] C. Dwyer, M. Weyland, L.Y. Chang and B.C. Muddle, Appl. Phys. L. 98 (2011) p. 201909. doi:10.1063/1.3590171.
[62] C.D. Marioara, W. Lefebvre, S.J. Andersen and J. Friis, J. Mater. Sci. 48 (2013) p. 3638. doi:10.1007/s10853-013-7158-3.
[63] A. Bendo, K. Matsuda, S. Lee, K. Nishimura, N. Nunomura, H. Toda, M. Yamaguchi, T. Tsuru, K. Hirayama, K. Shimizu, H. Gao, K. Ebihara, M. Itakura, T. Yoshida and S. Murakami, J. Mater. Sci. (2017) doi:10.1007/s10853-017-1873-0.
[64] S. Wenner, J. Friis, C.D. Marioara and R. Holmesta, J. All. Comp. 684 (2016) p. 195. doi:10.1016/j.jallcom.2016.05.132.
[65] D. Schechtman, I. Blech, D. Gratias and J.W. Cahn, Phys. Rev. Lett. 53 (1984) p. 1951. doi:10.1103/PhysRevLett.53.1951.
[66] W. Steurer, Z. Kristallogr. 219 (2004) p. 391.
[67] M. Audier and P. Guyot, *Aperiodicity and Order 3: Extended Icosahedral Structures*, Academic Press, San Diego, 1989.

[68] L. Zhen, W.D. Fei, S.B. Kang and H.W. Kim, J. Mater. Sci. 32 (1997) p. 1895. doi:10.1023/A:1018569226499.
[69] J. Zhang, Y.N. Huang, C. Mao and P. Peng, Sol. State Comm. 152 (2012) p. 2100. doi:10.1016/j.ssc.2012.09.003.
[70] S.P. Ringer, B.T. Sofyan, K.S. Prasad and G.C. Quan, Acta Mater. 56 (2008) p. 2147. doi:10.1016/j.actamat.2007.12.046.
[71] Z. Liang, *Clustering and Precipitation*. *PhD thesis* HZB-B38 Institut für Angewandte Materialforschung, Helmholz-Zentrum Berlin, Germany, 2012, doi: 10.5442/d0032
[72] G.A. Edwards, K. Stiller, G.L. Dunlop and M.J. Couper, Acta. Mater 46 (1998) p.3893.
[73] K. Matsuda, Y. Sakaguchi, Y. Miyata, Y. Uetani, T. Sato, A. Kamio and S. Ikeno, J. Mater. Sci. 35 (2000) p. 179. doi:10.1023/A:1004769305736.
[74] N.A. Bul'enkov, A.G. Yakovenko and O.M. Ul'yanikhina, J. Struct. Chem. 11 (1971) p. 1059. doi:10.1007/BF00744614.
[75] S.J. Andersen, C.D. Marioara, R. Vissers, A.G. Frøseth and H.W. Zandbergen, Mat. Sci. Eng. A. 444 (2007) p. 157. doi:10.1016/j.msea.2006.08.084.
[76] H.W. Zandbergen, S.J. Andersen and J. Jansen, Science. 277 (1997) p. 1221. doi:10.1126/science.277.5330.1221.
[77] S.J. Andersen, C.D. Marioara, A.G. Frøseth, R. Vissers and H.W. Zandbergen, Mat. Sci. Eng. A. 390 (2005) p. 127. doi:10.1016/j.msea.2004.09.019.
[78] K. Teichmann, C.D. Marioara, S.J. Andersen and K. Marthinsen, Metall. Mater. Trans. A. 43 (2012) p. 4006. doi:10.1007/s11661-012-1235-0.
[79] R. Vissers, M.A. van Huis, J. Jansen, H.W. Zandbergen, C.D. Marioara and S.J. Andersen, Acta Mater. 55 (2007) p. 3815. doi:10.1016/j.actamat.2007.02.032.
[80] R. Vissers, C.D. Marioara, S.J. Andersen and R. Holmestad, Aluminium Alloys. 2 (2008) p. 1263.
[81] S.D. Dumolt, D.E. Laughlin and J.C. Williams, Scr. Metall. 18 (1984) p. 1347. doi:10.1016/0036-9748(84)90362-4.
[82] M. Torsæter, F.J.H. Ehlers, C.D. Marioara, S.J. Andersen and R. Holmestad, Phil. Mag. 92 (2012) p. 3833. doi:10.1080/14786435.2012.693214.
[83] L. Arnberg and B. Aurivillius, Acta Chem. Scand. A. 34 (1980) p. 1. doi:10.3891/acta.chem.scand.34a-0001.
[84] C.D. Marioara, S.J. Andersen, J. Friis, O. Engler, and Y. Aruga, *The nature of solute clusters and GP-zones in the Al-Mg-Si system*. The proceedings of the 16th International Aluminum Alloys Conference (ICAA16), McGill University, Montreal, QC, 2018, June 17–19. ISBN: 978-1-926872-41-4.
[85] T. Saito, E.A. Mørtsell, S. Wenner, C.D. Marioara, S.J. Andersen, J. Friis, K. Matsuda and R. Holmestad, Adv. Eng. Mater. (2018) p. 1800125. doi:10.1002/adem.201800125.
[86] L. Kovarik, S.A. Court, H.L. Fraser and M.J. Mills, Acta Mater. 56 (2008) p. 4804. doi:10.1016/j.actamat.2008.05.042.
[87] L. Kovarik and M.J. Mills, Scripta Mater. 64 (2011) p. 999. doi:10.1016/j.scriptamat.2011.01.033.
[88] Z.R. Liu, J.H. Chen, S.B. Wang, S.W. Yuan, M.J. Yin and C.L. Wu, Acta. Mater. 59 (2011) p. 7396. doi:10.1016/j.actamat.2011.08.009.
[89] H.S. Hasting, A.G. Frøseth, S.J. Andersen, R. Vissers, J.C. Walmsley, C.D. Marioara, F. Danoix, W. Lefebvre and R. Holmestad, J. Appl. Phys. 106 (2009) p. 123527. doi:10.1063/1.3269714.

[90] P.H. Ninive, A. Strandlie, S. Gulbrandsen-Dahl, W. Lefebvre, C.D. Marioara, S.J. Andersen, J. Friis, R. Holmestad and O.M. Løvvik, Acta Mater. 69 (2014) p. 126. doi:10.1016/j.actamat.2014.01.052.
[91] S. Wenner, L. Jones, C.D. Marioara and R. Holmestad, Micron. 96 (2017) p. 103. doi:10.1016/j.micron.2017.02.007.
[92] G.A. Edwards, K. Stiller, M.J. Couper and G.L. Dunlop, Mater. Sci. For. 217-222 (1996) p. 713.
[93] T. Saito, C.D. Marioara, S.J. Andersen, W. Lefebvre and R. Holmestad, Phil. Mag. 94 (2014) p. 520. doi:10.1080/14786435.2013.857051.
[94] M.A. van Huis, M.H.F. Sluiter, J.H. Chen and H.W. Zandbergen, Phys. Rev. B. 76 (2007) p. 174113. doi:10.1103/PhysRevB.76.174113.
[95] K. Li, A. Béche, M. Song, G. Sha, X. Lu, K. Zhang, Y. Du, S.P. Ringer and D. Schryvers, Scripta Mater. 75 (2014) p. 86. doi:10.1016/j.scriptamat.2013.11.030.
[96] X. Pang, W. Yang, J. Yang, M. Pang and Y. Zhan, Intermetallics. (2017) (In press) . doi:10.1016/j.intermet.2017.10.014.
[97] B. Heying, R.D. Hoffmann and R. Pöttgen, Z. Naturforsch. 60B (2005) p. 491.
[98] W.F. Miao and D.E. Laughlin, Met. Mater. Trans. A. 31 (2000) p. 361. doi:10.1007/s11661-000-0272-2.
[99] M. Murayama, K. Hono, W.F. Miao and D.E. Laughlin, Met. Mater. Trans. A. 32 (2001) p. 239. doi:10.1007/s11661-001-0254-z.
[100] D.J. Chakrabarti, Y. Peng and D. Laughlin, Mater. Sci. For. 396-402 (2002) p. 857.
[101] C.D. Marioara, S.J. Andersen, T.N. Stene, H. Hasting, J. Walmsley, A.T.J. van Helvoort and R. Holmestad, Phil. Mag. 87 (2007) p. 3385. doi:10.1080/14786430701287377.
[102] C. Cayron, L. Sagalowicz, O. Beffort and P.A. Buffat, Philos. Mag. A. 79 (1999) p. 2833. doi:10.1080/01418619908212027.
[103] S.J. Andersen, C.D. Marioara, R. Vissers, A. Frøseth and P. Derlet, Proc. EMC 2000. 2 (2004) p. 599.
[104] F.J.H. Ehlers, S. Wenner, S.J. Andersen, C.D. Marioara, W. Lefebvre, C.B. Boothroyd and R. Holmestad, J. Mater. Sci. 49 (2014) p. 6413. doi:10.1007/s10853-014-8371-4.
[105] C. Cayron and P.A. Buffat, Acta Mater. 48 (2000) p. 2639. doi:10.1016/S1359-6454(00)00057-4.
[106] L. Ding, Z. Jia, J.-F. Nie, Y. Weng, L. Cao, H. Chen, X. Wu and Q. Liu, Acta Mater. 48 (2018) p. 2639.
[107] C.D. Marioara, J. Nakamura, K. Matsuda, S.J. Andersen, R. Holmestad, T. Sato, T. Kawabata and S. Ikeno, Philos. Mag. 92 (2012) p. 1149. doi:10.1080/14786435.2011.642319.
[108] R. Bjørge, C.D. Marioara, S.J. Andersen and R. Holmestad, Metall. Mater. Trans A. 41 (2010) p. 1907. doi:10.1007/s11661-010-0301-8.
[109] R. Bjørge, P.N.H. Nakashima, C.D. Marioara, S.J. Andersen, B.C. Muddle, J. Etheridge and R. Holmestad, Acta Mater. 59 (2011) p. 6103. doi:10.1016/j.actamat.2011.06.021.
[110] R. Bjørge, S.J. Andersen, C.D. Marioara, J. Etheridge and R. Holmestad, Philos. Mag. 92 (2012) p. 3983. doi:10.1080/14786435.2012.700129.